JOURNAL OF AIRCRAFT
Vol. 34, No. 5, September–October 1997

Development of Vortical Structure over Delta Wing with Leading-Edge Flap

Cheng-Hsiung Kuo* and C. W. Hsu†
National Chung-Hsing University, Taichung 40227, Taiwan, Republic of China

Development of a vortical structure over a delta wing with an oscillating leading-edge flap is studied experimentally. The base delta wing has a 60-deg sweep-angle and was inclined at 25 deg angle of attack. The width of the leading-edge flap varies from the apex to the trailing edge of the wing, forming a triangular shape of 5-deg apex angle. As the leading-edge flap is deflected statically on the windward side, the flow structure strongly depends upon the angle of attack and the flap deflection angle. Significant delay of the vortex breakdown location can be attained while the time scale (or the period) of the oscillating leading-edge flap is close to one convection time scale. When the oscillating leading-edge flap has a period much shorter than the convection time scale, the effectiveness in delaying the vortex breakdown location is reduced. Meanwhile, the development of vortex breakdown experiences a certain amount of time delay (or phase shift). Mutual interaction between vortical structures over the wing surface is found to be the key mechanism for this time delay.

Nomenclature

C	=	root chord of the delta wing, 20 cm
F	=	apex angle of the linearly tapered leading-edge flap, 5 deg
f_e	=	flap oscillation frequency, $1/T_e$
f^*	=	reduced frequency, f_eC/U_0
Re_C	=	Reynolds number based on the root chord, U_0C/ν
s	=	local semispan at any x/C location
S_0	=	semispan at $x/C = 1.0$
T	=	thickness of the wing
Te	=	flap oscillation period, $1/f_e$
t^*	=	dimensionless time, t/Te
U_c	=	centerline velocity of the vortex core
U_c^*	=	normalized center velocity, U_c/U_0
U_0	=	uniform inflow velocity, 7.5 cm/s
X_b	=	core length prior to vortex breakdown
X_{bm}	=	maximum core length prior to breakdown
X, Y, Z	=	coordinate system fixed on the vortex core, Fig. 1
x, y, z	=	laboratory coordinate system, Fig. 1
α	=	angle of attack of the wing
Γ	=	local circulation at $x/C = 0.6$
Γ^*	=	dimensionless circulation, Γ/CU_0
Λ	=	sweep angle of the delta wing, Fig. 1c
ϕ	=	deflection angle of the flap, Fig. 1c

Introduction

THE highly swept delta wing continues to be an important focus of research, because it defines high lift at a wider angle-of-attack (AOA) range. During maneuvering phases such as landing, takeoff, initial climb, etc., the delta wing aircraft often operates at subsonic speed and high AOA. Unlike the stall phenomenon that occurs over the two-dimensional airfoil, the formation of a stable leading-edge vortex structure induces a strong suction peak on the leeward surface of the delta wing at higher AOA. At high AOA, the stable leading-edge vortical structure above the delta wing not only produces high lift, it also contributes a large amount of drag to the wing.[1] Therefore, a penalty is paid in the form of poor aerodynamic efficiency such as low lift/drag (L/D) ratio.

Study of the stable leading-edge vortex and the associated vortex breakdown is also important not only for controlling stability in yaw and in roll,[2,3] but also for suppressing unsteady buffeting.[4] Active and passive control techniques have been developed for stable and safe flight.[5–8] Two kinds of control techniques are available.

1) Blowing in the spanwise and along the vortex core directions accelerates the vorticity convection downstream. The high lift induced by stronger suction pressure distribution and the significant delay of vortex breakdown have been explored.[9–12]

2) Control of vorticity generation by modifying the shear-layer structure separated from the leading edge provides diversified means (either active or passive) to enhance the lift or aerodynamic performance.[1,13–16]

In past years, the leading-edge flap has been used with the two-dimensional airfoil for lift enhancement by introducing unsteadiness.[17] The concept of a leading-edge flap used with delta wings was suggested by Lamar and Campbell[18] as the second kind of advanced control device. Detailed discussions on the potential applications of the vortex flap are given in their paper.[18] Several investigations reveal that an upward-deflected flap is useful mainly to enhance the lift at zero and low-to-moderate AOA.[1,15] At high AOA, both the lift and the drag forces increase, leading to a small L/D ratio. Recently, Deng and Gursul[19] studied the flowfield over the upward-deflected static flap. In this study, both the vortex breakdown location and its sensitivity to the AOA and the flap deflection angle are reported. These are related to the details of the shear-layer structure, the axial and swirling velocity, and the swirling angle.

On the other hand, the downward-deflected flap is usually used to reduce the drag, leading to a higher L/D ratio. Several investigations have focused on understanding the unsteady loading, the surface pressure distribution on the wing and on the flap, as well as the L/D ratio.[13–16] The conclusion has been that the proper size and deflection angle of the leading-edge flap will cause the formation of a leading-edge vortex over the flap surface. In this situation, a thrust force is produced on the flap surface while the vortex lift is still maintained, resulting in high L/D ratio. An overview on the research of the leading-edge vortex flap is provided by Campbell and Osborn,[20] discussing the challenges of these devices.

Received Dec. 2, 1996; revision received May 5, 1997; accepted for publication May 6, 1997.

*Associate Professor, Department of Mechanical Engineering.
†Graduate Student, Department of Mechanical Engineering.

Most of the previous studies focused on the effect of the static leading-edge flap on the unsteady loading and the surface pressure distribution. Detailed information on both the flow structure and the controlling parameters remain incomplete. In this study, a downward-deflected flap is used to oscillate harmonically in an attempt to both increase the lift and reduce the drag. It is intended to realize the sensitivity of the vortex breakdown location to the AOA and the flap deflection angle. Furthermore, the development of vortex breakdown within the oscillation cycle is examined while the downward deflected leading-edge flap oscillates at a small amplitude (±1 deg).

In the present study, the base wing (half delta wing) has a 60-deg sweep angle with a downward-deflected leading-edge flap. A one-component laser Doppler anemometry (LDA) system is used to explore the unsteady flow characteristics. On the cross-sectional plane at $x/C = 0.6$, a modified phase-averaged technique is employed to reconstruct the instantaneous flow pattern at selected instants within the oscillation cycle. The patterns reveal the mutual interaction among the vortex structures over the wing.

Experimental Setup

Operation Conditions

All experiments were performed in a low-speed recirculation water channel, whose dimensions are 40 cm by 40 cm square and 250 cm in length. Several sizes of fine mesh and honeycomb are installed upstream of the contraction to reduce turbulence intensity down to a level of 0.41% at $Re_C = 1.5 \times 10^4$ for all experimental conditions. Considering the least-square analysis of the freestream velocity measurement, the nonuniformity across the test section is about 0.87%. Visualization of the vortical flow patterns over the wing surface and the leading-edge flap is performed for 15 deg ≤ α ≤ 30 deg; whereas the leading-edge flap is statically deflected on the windward side at different deflection angles ϕ. However, in case of the flap oscillating about ϕ = 60 deg, the oscillating amplitude is ±1 deg, and the reduced frequency varies between 1.2–5.9 for α = 25 deg.

Coordinate System and Model Geometry

As depicted in Figs. 1a and 1b, x, y, and z define the laboratory coordinate system; whereas X, Y, and Z denote the coordinate system fixed to the vortex core. The cross-sectional plane of axial velocity contour measurement is selected at $x/C = 0.6$. However, U_c^* and the local circulation measurements are selected at $x/C = 0.5$, where vortex breakdown does not occur. In Fig. 1c, the half delta wing model has 60-deg sweep angle and is beveled upward on the windward side, forming a sharp leading edge. The thickness to root chord ratio T/C of the wing is about 2.5%, so that it can be considered as a thin wing. Furthermore, the leading-edge oscillating flap is tapered from the wing apex to the trailing end of the wing to form a triangular shape having a flap angle $F = 5$ deg. The thickness of the flap is about $0.31\%C$, ensuring a flap of sharp leading edge. The angle ϕ of the leading-edge flap is defined to be positive while the flap is deflected on the windward side (or downward deflected flap).

Figure 2 shows the installation of the half delta wing model and the driving mechanism for simple harmonic oscillation of the leading-edge flap. The AOA can be adjusted simply by screwing each hole to the wing model with the wing tip being a rotating center. The half delta wing model sits on the full-span horizontal platform having a leading-edge of 5:1 elliptic profile. The blockage ratio of the half-wing model is around 3.1% for α = 30 deg, ensuring minimum distortion of the flow caused by insertion of the model. Details of the model arrangements on the platform can be found by referring to Kuo and Lu.[11]

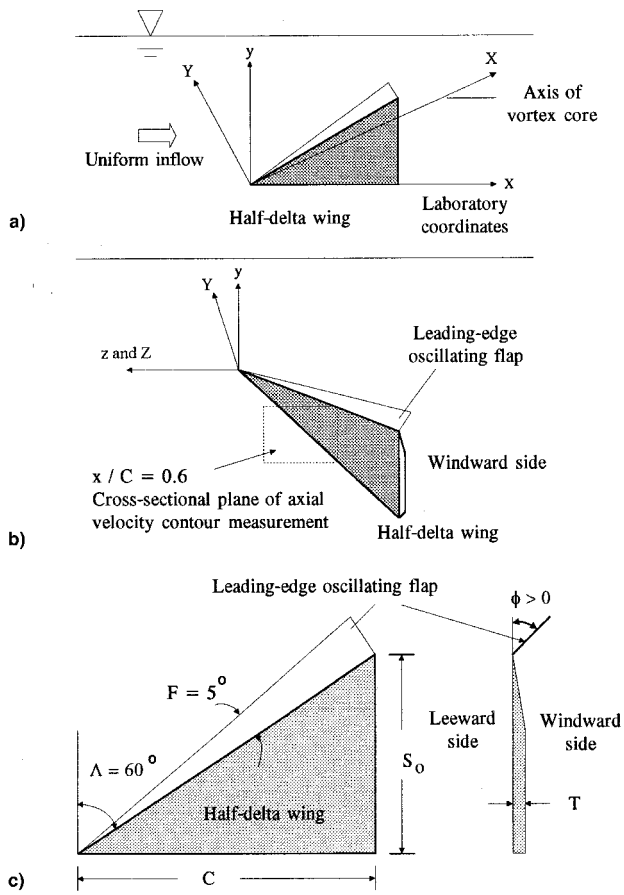

Fig. 1 Coordinate systems and the geometric configuration of the half delta wing.

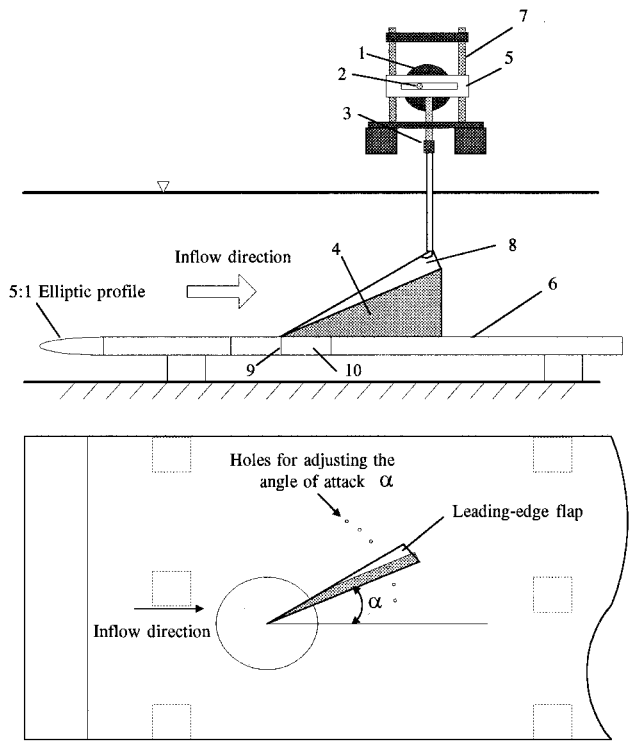

Fig. 2 Installation of the half delta wing model, the simple harmonic oscillating leading-edge flap, and its driving mechanism. 1, Simple rotating disk; 2, eccentric driving roller; 3, adapter for transmitting the simple harmonic motion; 4, half delta wing model; 5, sliding bar; 6, supporting platform; 7, guiding rails; 8, leading-edge oscillating flap; 9, dye injection pinhole; and 10, fit-in circular disk.

Oscillating Mechanism

Oscillation of the leading-edge flap is driven by the mechanism shown in Fig. 2 that generates the simple harmonic motion. In fact, pure rotation of the simple rotating disk (labeled as 1) is driven by a dc motor. This purely rotating motion is transmitted by the driving roller (labeled as 2), mounted eccentrically on the simple rotating disk. By the arrangements of a sliding bar and a pair of guiding rails (labeled as 5 and 7), the pure rotation of element 1 can be converted into a simple harmonic reciprocating motion. The oscillating amplitude can be adjusted simply by changing the eccentricity of the driving roller. This mechanism, that generates only a single frequency, provides a good reference for triggering the data acquisition at the phase of maximum $\phi = 61$ deg. This technique is crucial to show the development of the unsteady flow structures during the oscillation cycle.

Visualization Technique and Velocity Measurements

The flow patterns on both the plane and the end views can be visualized by casting the laser light sheet on the flow domain. Fluorescent dye, flowing naturally from a tiny slot very close to the wing apex, was introduced to reveal the vortex core and the associated breakdown location. Instantaneous vortex breakdown location of the primary vortex can be read precisely by playing back in the time-base corrected mode at a rate of 30 frames/s. The results shown in Figs. 4 and 6 are the averaged value over 15 flap oscillation cycles recorded from the video tape.

Velocity measurement for the axial velocity is taken on the cross-sectional plane at $x/C = 0.5$ and 0.6, where the vortex core does not break down. Axial (or along the vortex core) velocity component is measured point-by-point through the one-component backscattered LDA system together with a precise traversing table. The LDA system contains an Ar + laser source, a Bragg cell for frequency shifting, and an integrated optic-fiber-based detecting and receiving module. The correlation-based signal processor is employed for data acquisition. By using a beam expander, the size of the measuring volume is 0.043 mm in diameter and 0.51 mm in length. The standard deviation of velocity measurement in uniform stream is around 0.73%. There are around 500 measuring points on the specific planes at $x/C = 0.5$ and 0.6 to provide sufficient spatial resolution. Within the flow domain, reconstruction of the instantaneous spatial distribution of the flow structures can be achieved by a modified version of the phase-averaging technique.[21] The phase-averaged instantaneous flow patterns can illustrate the interactions among the organized vortical flow structures within the oscillation cycle. Furthermore, this technique is also applied to evaluate the cyclic variation of the local circulation at $x/C = 0.5$ along the contour B depicted in the inset of Fig. 5. The contour B is chosen so that both the swirling velocity and its radial gradient are nearly zero across the boundaries (dashed lines in Fig. 5). Among the measuring points within the flow domain, the maximum standard deviation from the phase-averaged axial velocity within the oscillation cycle is 2.7%. However, the variation in the period of the oscillation cycle is only 0.96%. These results confirm that the vortical flow structure is quite periodic with very little time shift and amplitude distortion. Therefore, the instantaneous vortex patterns reconstructed by the modified phase-averaged technique can faithfully reveal the flow structure and thereby capture the interacting mechanism.

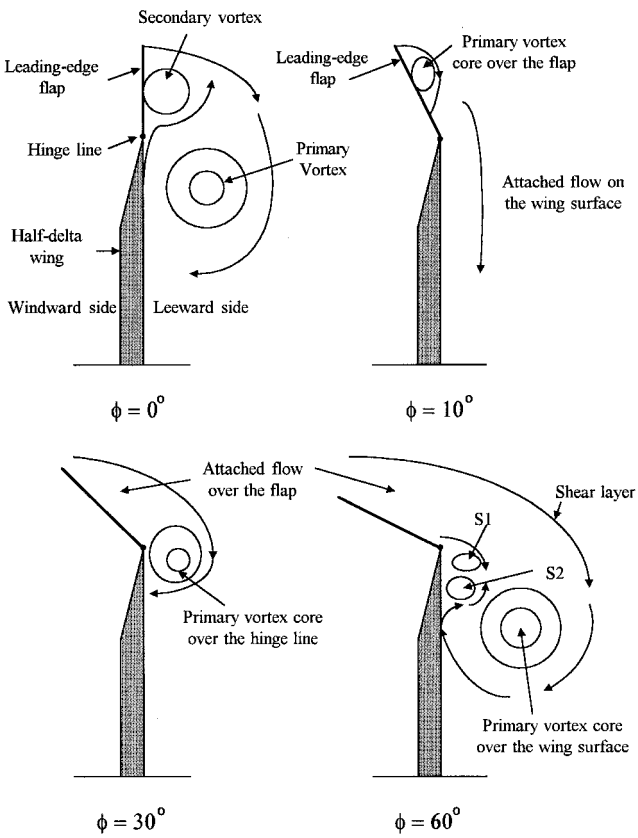

Fig. 3 Typical end view flow patterns over the leading-edge flap and the wing surface at different deflection angles on the windward side for AOA = 25 deg. Note that the end views shown here and in Fig. 8 are the views from flow visualization by a downstream reflecting mirror. These views are the exact mirror images of that shown in Fig. 1c.

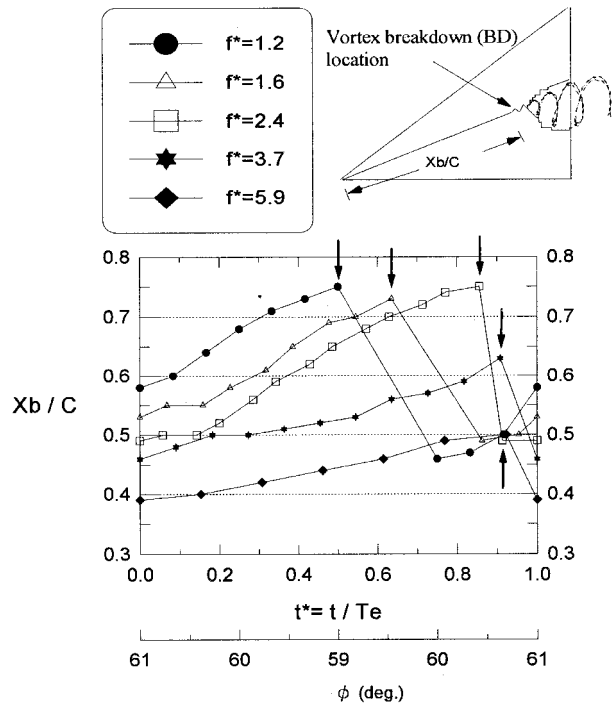

Fig. 4 Instantaneous onset locations of the vortex breakdown within the flap oscillation cycle at different oscillating frequencies. It shows the development of vortex breakdown when AOA = 25 deg and flap deflection angle changes from 61 to 59 deg. The maximum deviation of the X_b/C over 15 oscillation cycles is around 3.0%. $X_b/C = 0$ at the wing apex.

Results and Discussions

Flow Structure for Statically Deflected Flap

As depicted in Fig. 6, the length of the vortex core prior to breakdown is presented for 0 deg $\leq \phi \leq$ 90 deg and 15 deg $\leq \alpha \leq$ 30 deg. For fixed ϕ of the flap, an increase in AOA causes an increase in the swirling velocity and a reduction in

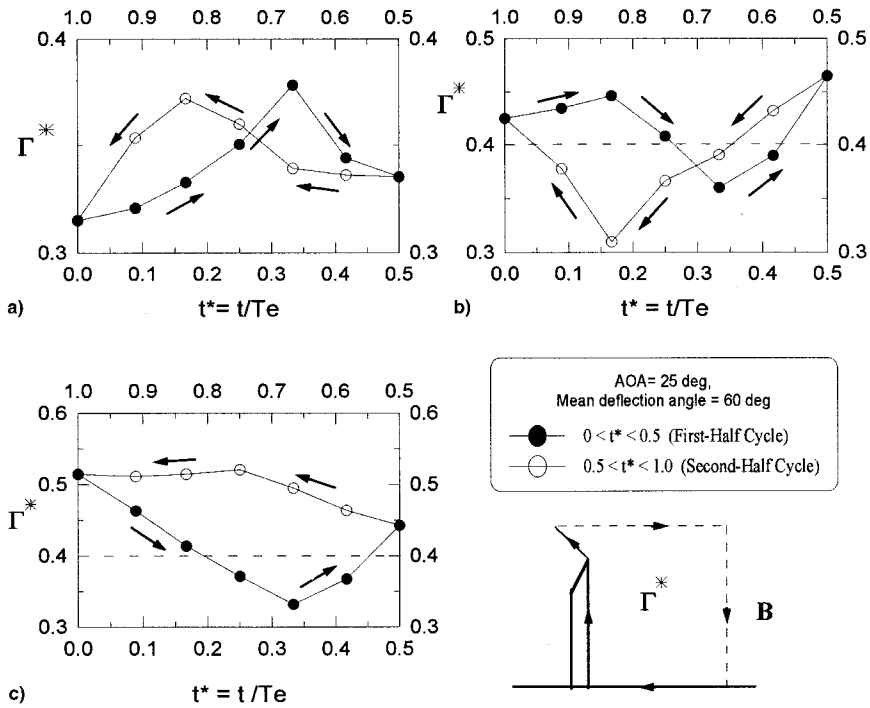

Fig. 5 Cyclic variations of the normalized local circulation show the hysteresis character at three reduced frequencies: f^* = a) 3.7, b) 2.4, and c) 1.2. The solid circles represent the first-half cycle. The open circles denote the second-half cycle. The inset shows the line contour for evaluating the local circulation at each instant. Maximum deviation among the instants within the oscillation cycle is 3.7%. The measurements are taken at x/C = 0.5, where vortex breakdown does not occur.

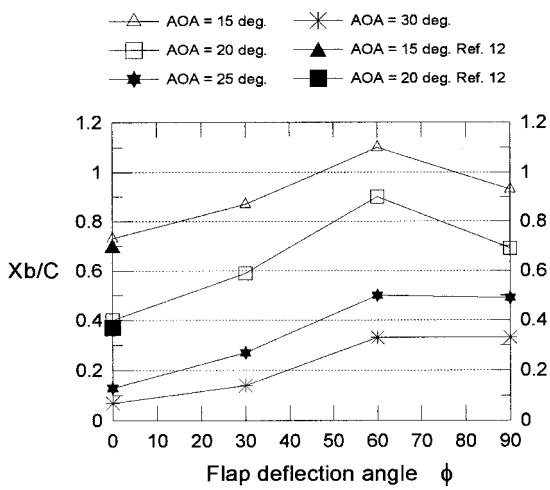

Fig. 6 Mean (long-time averaged) breakdown location of the primary vortex at different AOA as the leading-edge flap is stationary at various deflection angles on the windward side. The data in Ref. 12 have 55-deg sweep angle. The maximum deviation of X_b/C is about 2.1% of the root chord.

the axial (or along-core) velocity. Considering the vorticity balance concept,[22] a higher swirling velocity at the leading edge of the flap will generate a large amount of vorticity that feeds into the primary vortex core. Reduction of the axial (or along-core) velocity slows down the vorticity convection. This imbalance of vorticity between the vorticity generation and downstream convection will lead to premature vortex breakdown. Therefore, the length of the vortex core prior to breakdown decreases as the AOA increases. On the other hand, for fixed AOA, the effective sweep angle of the delta wing (including the deflected flap) decreases while the deflection angle of the leading-edge flap decreases; e.g., change from ϕ = 60 to 0 deg. A reduction of the sweep angle induces lower along-core velocity that slows down the vorticity convection, leading to early breakdown of the primary vortex core. Therefore, the effectiveness of delaying the vortex breakdown location becomes pronounced at large deflection angle up to ϕ = 60 deg. For all of the AOA studied herein, the vortex core length reaches its maximum at ϕ = 60 deg. Among the maximums at ϕ = 60 deg, α = 15 and 20 deg are the two most effective cases to delay the vortex breakdown location. For example, for α = 15 deg, the core length increases about 50% at ϕ = 60 deg compared with that at ϕ = 0 deg. More significantly, the core length becomes 2.25 times that of ϕ = 0 deg for α = 20 deg.

The end-view flow patterns at different AOA and various flap deflection angles are studied extensively by the laser sheet technique. Typical flow structures are sketched in Fig. 3 at a selected deflection angle ϕ for α = 25 deg. In case of ϕ = 0 deg, the half-wing configuration becomes a simple delta wing with 55-deg sweep angle. Apart from the primary vortex core over the wing surface, there is a secondary vortex over the leading-edge flap because of the boundary-layer separation in the spanwise direction. The results obtained at ϕ = 0 deg are very close to the previous study[12] (see Fig. 6). This further confirms that the setup and flow condition of the half delta wing model are not far apart from the complete delta wing.

When the deflection angle of the leading-edge flap on the windward side is small (e.g., ϕ = 10 deg), a small vortex core can be found only over the leading-edge flap. Over the majority of the wing surface, the flow is found to be attached. The attached flow over the wing surface is primarily caused by a positive-camber effect that is induced by the downward- (or windward-) deflected leading-edge flap. As the deflection angles of the leading-edge flap further increase up to $\phi \approx 30$ deg, the primary vortex core moves inboard and is located over the hinge line. At even higher deflection angle ϕ = 60 deg, the scale of the primary vortex core becomes significant and moves further inboard over the wing surface. There are two small-scale vortices (S1 and S2) near the hinge line. The structure S1 is caused by the boundary-layer separation from the hinge line. However, the structure S2 corresponds to the secondary vortex caused by the spanwise boundary-layer separation from the wing surface. The flow structures in Fig. 3 also

coincide with some of the surface pressure distributions measured on the wing and flap surfaces.[14] At $\phi = 60$ deg, the flow over the flap is attached to the flap surface because the downward deflected flap is facing the incoming flow at $\alpha = 25$ deg. In fact, the flow over the flap is also very sensitive to the apex angle F and the size of the flap, the AOA, the sweep angle, etc. This investigation is currently underway.

As a limiting case, $\phi = 90$ deg, the S1 structure overwhelms the S2 structure and provides strong interactions with the primary vortex core (not shown here). This mechanism is responsible for the adverse effect on delaying the vortex breakdown location while the deflection angle is 90 deg.

Phase Shift at Different Reduced Frequency

In studying the dynamic characteristics of the vortex core, the plane view is also employed to qualitatively illustrate the development of the vortex breakdown location in response to the harmonic flap motion. Flap motion can be expressed in terms of $\phi(t) = 60 \text{ deg} + 1 \text{ deg} \cos(2\pi f_e t)$. It oscillates periodically about $\phi = 60$ deg, and has a small amplitude, ± 1 deg. $f^* = f_e C/U_0$ is selected within $1.2 \leq f^* \leq 5.9$ in an attempt to generate stronger vortex through the flap oscillation.

In the present study, vortex breakdown is of the spiral type. The primary vortex core takes the form of a nearly straight line before breakdown. It starts to deviate from this stable position by the appearance of a small oscillation. About $0.04C$ downstream of this location, the vortex core diffuses rapidly in a spiral manner. Therefore, identifying the onset location of a bubble-type breakdown by the abrupt divergence of the vortex core is not suitable. For a spiral-type breakdown, the onset of vortex breakdown is defined as the location where the small oscillation occurs, shown in the inset of Fig. 4.

Figure 4 shows the instantaneous onset locations X_b/C of vortex breakdown and its development during the flap oscillation cycle for $\alpha = 25$ deg and $1.2 \leq f^* \leq 5.9$. The general trend of the onset location of vortex breakdown is initially pushed downstream during a certain part of the oscillation cycle. However, it moves upstream rather quickly within the rest of the oscillation cycle. When the flap is at $\phi = 61$ deg (or $t^* = 0$), the downstream development of the breakdown location takes a certain time delay to reach the maximum value (as indicated by arrows) for each reduced frequency. The amount of the time delay (or phase shift) increases and becomes significant as the reduced frequency increases. For example, the time delay (or phase shift) at $f^* = 1.2$ is around $0.5Te$. However, the time delay is almost $0.82Te$ at $f^* = 2.4$. For the limiting cases $f^* \geq 3.7$, the amount of time delay approaches $0.9Te$ asymptotically. Obviously, the cyclic development of vortex breakdown will take different amounts of time delay (or phase shift) to attain the longest core length when the leading-edge flap oscillates at different reduced frequencies. A similar time delay (or phase shift) in the unsteady lift within the oscillation cycle can also be found in Huyer et al.,[23] for a harmonically oscillating simple delta wing with a 45-deg sweep angle.

Frequency Response

In addition to the time delay (or phase shift) shown in Fig. 4, the farthest breakdown locations (X_{bm}/C) of the primary vortex core are shown as functions of the reduced frequency of the oscillating flap. In Fig. 7, X_{bm}/C has the maximum value for $1.2 \leq f^* \leq 2.4$ and it reduces significantly for $f^* > 2.4$. As a limiting case, $f^* = 5.9$, the farthest breakdown location (X_{bm}/C) of the primary vortex is only about $0.5C$. At the highest reduced frequency studied herein, the core length is nearly the same as that of the static flap. This implies that the high-frequency (or small wavelength) perturbation does not significantly delay the vortex breakdown location. The effective delay of the vortex breakdown location occurs while the time scale (or period) of the external perturbation is close to the convection time scale C/U_∞. This result is similar to those in Refs. 24 and 11. This result is still not completely understood because the mechanism governing the vortex breakdown of the leading-edge vortex is still unclear. More work has to be done in this respect.

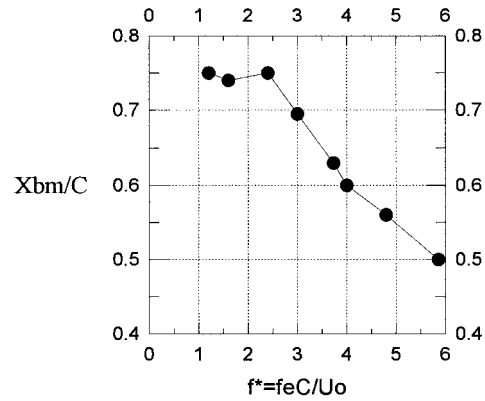

Fig. 7 Variations of the maximum core length prior to the vortex breakdown as functions of reduced frequency. The wing is at AOA = 25 deg, and the flap oscillates about the mean deflection angle (60 deg) with small amplitude (1 deg). The X_{bm}/C values are obtained from the farthest location in Fig. 4 for each reduced frequency.

Flow Structure at $x/C = 0.6$

Within the oscillation cycle, the phase-averaged flow structures over the delta wing are studied for $\alpha = 25$ deg and $\phi = 60$ deg while the flap oscillates at $f^* = 1.2$ and 2.4. The time-dependent flow structures are essentially similar except for the amount of time shift.[25] Therefore, only the instantaneous flow structures for $f^* = 2.4$ and $\alpha = 25$ deg are presented in Fig. 8 to illustrate the mutual interactions among the vortex flow structures over the delta-wing with a downward-deflected leading-edge flap.

In Fig. 8, the primary vortex structure is labeled as P. The SL denotes the shear-layer structure separating from the sharp leading edge of the oscillating flap. Both structures have the maximum value at the center of the contour with descending magnitude in the outward direction. However, the S structure represents the combination of S1 and S2 structures depicted in Fig. 3. It is characterized by high-contour values at the evolution front (e.g., the tongue-like structure adjacent to the upper-right of the P structure), but it is characterized by lower contour values near the hinge line. As for the L structure, it marks the footprint between the SL and P, forming a region of decreasing magnitude toward the center of the contours. Moreover, in the inset of Fig. 8, the path a–a denotes the first-half cycle of the flap oscillation. The labels 1, 2, and 3 represent the selected instants at $t^* = 1/6$, 2/6, and 3/6 while the flap motion follows the a–a path. Along the path b–b, the labels 4, 5, and 6 represent the instants at $t^* = 4/6$, 5/6, and 6/6 during the second half of the oscillation cycle. Recall that the oscillating amplitude of the flap is only ± 1 deg. In Fig. 8, the flap locations do not change with time because the flap motion is so small when all dimensions are on the same scale. However, the flap locations in the inset of Fig. 8 are exaggerated for easy illustration of the flap motion.

At the instant $t^* = 0$ (or $t^* = t/Te = 6/6$), the dominance of the S structure is clearly evidenced near the hinge line. Meanwhile, the SL structure is the strongest one because the flap is at the maximum deflection angle (e.g., $\phi = 61$ deg) on the windward side. At this instant, the contour of P still preserves the highly concentrated appearance, although it is severely distorted. Furthermore, the highly concentrated L structure clearly denotes the continuous supply of the vorticity that is feeding from SL into P.

Subsequently, at $t^* = 1/6$ following the a–a path, the growth of the S structure continues. The compactness of the L struc-

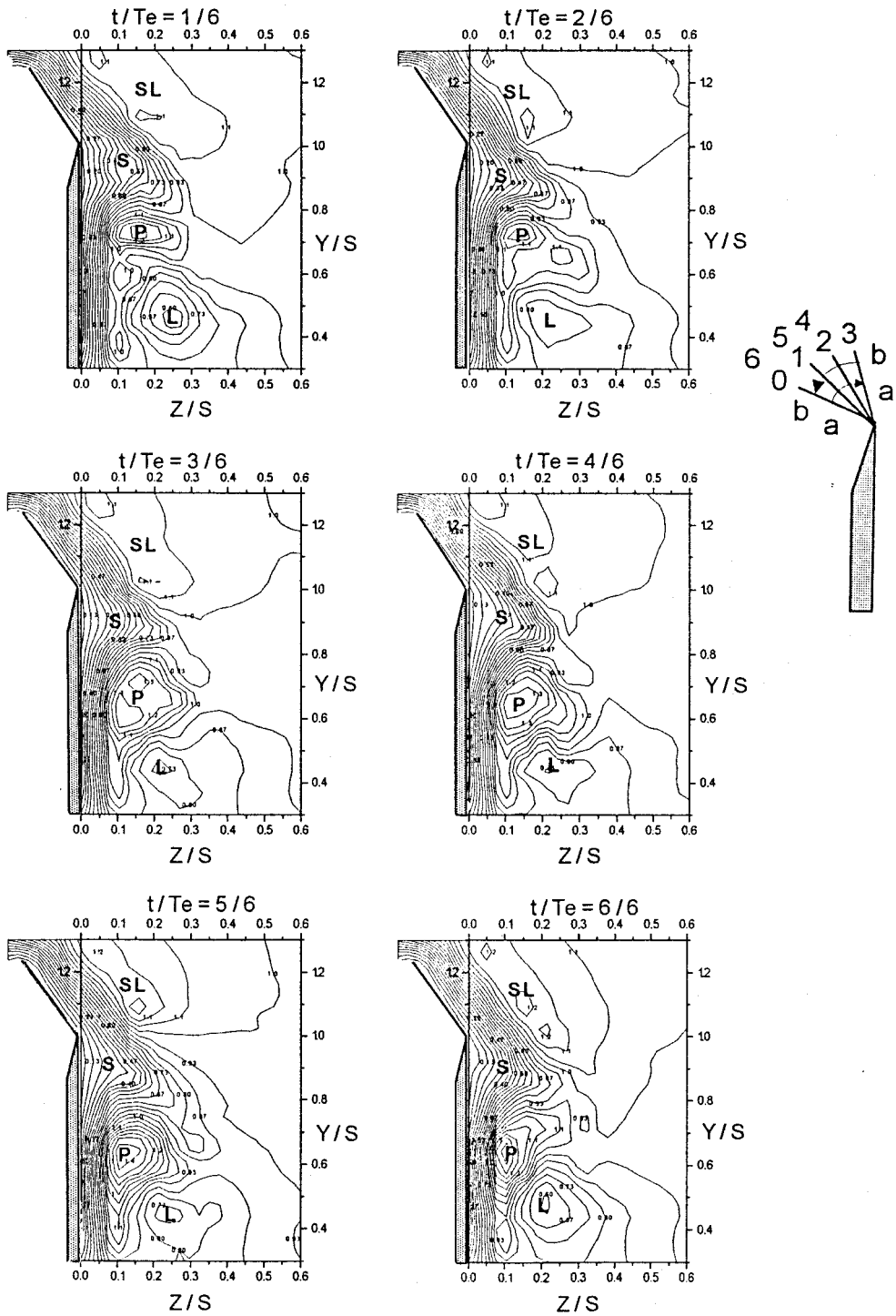

Fig. 8 Phase-averaged instantaneous contours of constant normalized axial velocity on the cross-sectional plane at $x/C = 0.6$ location at six selected instants within the flap oscillation cycle. It illustrates the interactions among the vortical structures while the flap oscillates at $f^* = 2.4$ for $\alpha = 25$ deg and $\phi = 60$ deg.

ture increases and P re-establishes its concentration, but the orientation is altered. This change further implies that the vorticity generated in the SL structure is continuously feeding into P. The feeding vorticity is carried by the small-scale highly concentrated eddies (or contours) that are situated between the L structure and the wing surface (the vertical shaded area). At $t^* = 2/6$, the appearance of the P structure becomes relatively diffused because it experiences severe distortion as a result of the continuous growth of the S structure closely adjacent to the top of the P structure. At $t^* = 3/6$, when the flap is at the minimum deflection angle ($\phi = 59$ deg), the SL structure is the weakest over the oscillation cycle. Despite the fact that the P structure is relatively diffused at this instant because of the overgrowth of the S structure, it still preserves the concentration to some extent. The relatively weak SL structure, in conjunction with the dominance and continuous growth of the S structure, will be responsible for the distorted and diffused primary vortex structure P during the first-half cycle.

Within $0.5 < t^* < 1.0$, following the b–b path, the flap tip moves in the opposite direction, resulting in an increase of the velocity gradient across the separated shear layer. This implies that the strength of the vorticity in SL structure starts to increase. At $t^* = 4/6$, the P structure re-establishes the highly concentrated feature with large gradient in the outward radial

direction. Within the interval $4/6 < t^* < 5/6$, the increasing concentration of the P structure indicates the reinforcement of the P structure. Meanwhile, the growth of the S structure (i.e., the tongue-like front) seems to slow down within the interval $3/6 < t^* < 5/6$. During the second-half cycle, both the enhanced strength of the shear-layer structure SL and the retarded growth of the S structure provide the opportunity for the primary vortex core P to reorganize. This substantially delays the onset location of the vortex breakdown near $t^* = 5/6$.

The shear layer (either the strength or the structures) will be modified by the oscillation flap. This causes a different vorticity generation (or supply) rate to the vortex core within the oscillation cycle. Throughout the cycle, a continuous vorticity supply into the primary vortex core favors the enhancement of the primary vortex structure P. However, the growth of the S structure leading to distortion of the primary vortex core P will have the adverse effect on the primary vortex core. Recall that, for $f^* = 2.4$, a reinforced P structure near $t^* = 5/6$ (Fig. 8) coincides with the substantial delay of the vortex breakdown at $t^* = 0.85$ (Fig. 4). This implies that the competition between the favorable and the adverse effects is the key mechanism. This mechanism primarily determines the time delay of the vortex breakdown while the downward (or windward) deflected leading-edge flap oscillates harmonically.

Centerline Velocity of Primary Vortex

To further realize the development of vortex breakdown within the oscillation cycle, the variations of the normalized centerline velocity U_c^* of the primary vortex core are presented in Fig. 9 for three different reduced frequencies. The measurement is taken at $x/C = 0.5$. In Fig. 9, the solid circles represent the instants within the first-half cycle, whereas the open circles denote the instants during the second-half cycle. The dashed line represents the centerline velocity U_c^* for the case of static flap ($f^* = 0$). The trend of the variation follows the indication of the arrows in Fig. 9. Within the oscillation cycle, all of the variations of the centerline velocity exhibit hysteresis character. However, the hysteresis loop at low reduced frequency $f^* = 1.2$ is in a reversed direction as those at higher reduced frequencies $f^* = 2.4$ and 3.7.

Within the oscillation cycle, the maximum centerline velocity occurs in the first-half cycle (e.g., $t^* = 0.42$) for $f^* = 1.2$. However, it occurs in the second-half cycle of the oscillation; e.g., $t^* = 0.66$ and $t^* = 0.75$, for $f^* = 2.4$ and 3.7, respectively. For each reduced frequency, the instants of maximum centerline velocity in Fig. 9 coincide roughly with those of the farthest breakdown locations in Fig. 4 with a certain amount of deviation. This is because the former (Fig. 9) exhibits only the local variation near the vortex center, and the latter (Fig. 4) reflects the global development of the vortex breakdown.

For a more precise description of vortex breakdown over a delta wing, both the axial and the swirling velocity components are important. Garg and Leibovich[26] showed that all flows result in vortex breakdown when the ratio of the maximum swirling velocity to the excess of the axial velocity exceeds a threshold value of around 1.5. In case of a leading-edge flap oscillating at high reduced frequency, strong interaction can be evidenced among the vortex structures (Fig. 8). The vortex core is severely distorted, leading to a nonsymmetric structure, and the maximum swirling velocity is difficult to identify in this situation. The magnitude of the local circulation represents the integral swirling effect within the flow domain at specified location $x/C = 0.5$. In case of the strong interacting flows (Fig. 8), the local circulation can be used to illustrate the development of the vortex core.

Variation of Dimensionless Circulation

The cyclic variations of the local circulation evaluated at $x/C = 0.5$ are presented in Fig. 5 for three different reduced frequencies. The dimensionless circulation is defined as $\Gamma^* = \Gamma/CU_0$, where Γ is evaluated by line integration along the contour B (the dashed line) shown in the inset of Fig. 5. The dashed line on each plot of Fig. 5 denotes the dimensionless local circulation for the case of static flap. Results in Figs. 4, 9, and 5 are to be cross-compared to show the relationships among the development of vortex breakdown, the local cir-

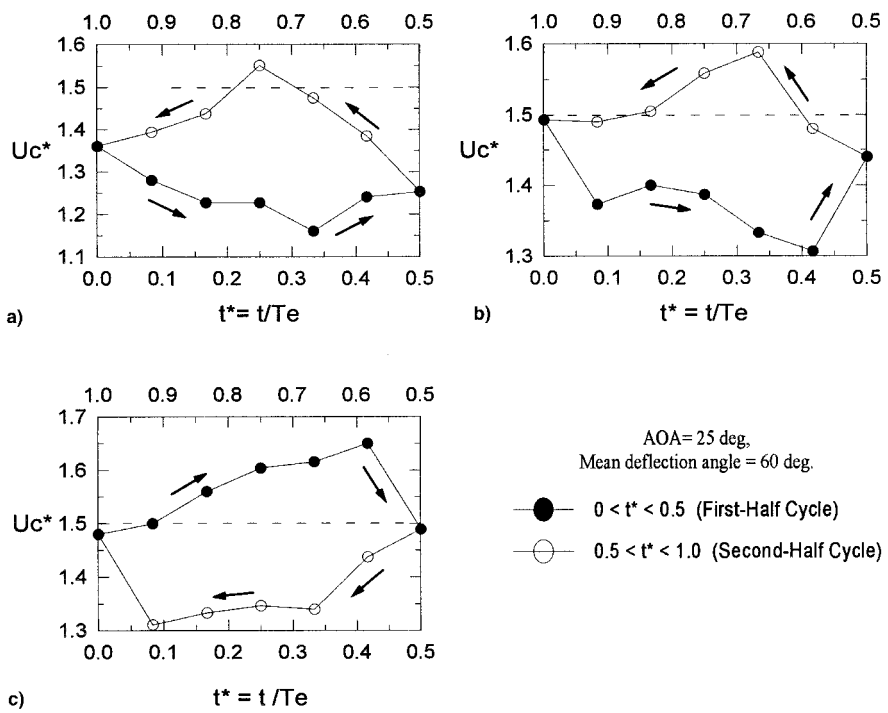

Fig. 9 Cyclic variations of the normalized axial velocity at the center of the vortex core for three reduced frequencies: f^* = a) 3.7, b) 2.4, and c) 1.2. The solid circles represent the first-half cycle. The open circles denote the second-half cycle. The maximum deviation of U_c^* among the instants within the oscillation cycle is 5.1%. The measurements are taken at $x/C = 0.5$, where the breakdown does not occur.

culation, and the variation of centerline velocity over the oscillation cycle.

In Fig. 5, the variations of Γ^* also exhibit the hysteresis character over the oscillation cycle for three different reduced frequencies. At $f^* = 1.2$, the hysteresis loop shows only a simple loop in counterclockwise direction. For $f^* = 1.2$, both the minimum circulation at $t^* = 0.33$ (Fig. 5a) and the maximum centerline velocity at $t^* = 0.42$ (Fig. 9a) induce the lowest Γ^*/U_c^* ratio near $t^* = 0.42$ during the first-half cycle of the oscillation. Both the maximum Γ^* at $t^* = 0.75$ and the minimum value of U_c^* at $t^* = 0.9$ lead to the highest value of Γ^*/U_c^* near $t^* = 0.833$. A low value of Γ^*/U_c^* implies (equivalent to the low ratio of swirling to axial-velocity excess in Ref. 26) longer vortex core prior to vortex breakdown location, whereas a higher value of Γ^*/U_c^* will lead to premature breakdown of the vortex core. These results clearly illustrate the time-dependent development of the vortex breakdown location shown in Fig. 4 for $f^* = 1.2$. However, at $f^* = 2.4$ and 3.7, their hysteresis loops have a similar ∞ shape, but with a certain amount of time delay. The minimum local circulation at $t^* = 0.83$ (Fig. 5b), together with the maximum centerline velocity at $t^* = 0.65$, leads to the minimum ratio Γ^*/U_c^* at $t^* = 0.83$ (during the second-half cycle) for $f^* = 2.4$. At $f^* = 1.2$ and 2.4, the flap oscillation increases both the U_c^* and the Γ^* over 70% of the cycle; whereas the U_c^* and the Γ^* values are smaller than that of the static case over 70% of the cycle at $f^* = 3.7$.

In Figs. 9 and 5, the instants corresponding to the lowest value of Γ^*/U_c^* at different reduced frequencies coincide with the instants of the farthest vortex breakdown locations shown in Fig. 4 within the oscillation cycle. This confirms that the time delay (or phase shift) of the vortex breakdown development is primarily caused by the mutual interaction between the vortical flow structures over the delta-wing. These results are true when the reduced frequency is higher than 1.2. However, for the reduced frequency lower than 1.2, no data are available in the present study because of the limitation of the oscillating mechanism.

Concluding Remarks

Development of the vortical structure over a delta wing with an oscillating leading-edge flap is studied experimentally. The base delta wing has 60-deg sweep-angle and was inclined at 25-deg angle of attack. The leading-edge oscillating flap varies from the apex to the trailing end of the wing, forming a triangular shape of 5-deg apex angle. As the leading-edge flap is deflected statically on the windward side, the flow structure strongly depends upon the angle of attack and the flap deflection angle. Significant delay of the vortex breakdown location can be attained while the time scale (or the period) of the oscillating leading-edge flap is near one convection time scale. Meanwhile, the development of the primary vortex core experiences a certain amount of time delay (or phase shift). Mutual interaction between vortical structures over the wing surface is found to be the key mechanism for this time delay.

Acknowledgment

The authors are grateful for the support of this work from the National Science Council of the Republic of China, Contract NSC-85-2212-E-005-006.

References

[1]Marchman, J. F., "Effectiveness of the Leading-Edge Vortex Flaps on 60 and 75 Degree Delta Wings," *Journal of Aircraft*, Vol. 18, No. 4, 1981, pp. 280–286.

[2]Rao, D. M., Moskovitz, C., and Murri, D. G., "Forebody Vortex Management for Yaw Control at High Angle of Attack," *Journal of Aircraft*, Vol. 24, No. 4, 1987, pp. 248–254.

[3]Ericsson, L. E., "Various Sources of Wing Rock," *Journal of Aircraft*, Vol. 27, No. 6, 1990, pp. 488–494.

[4]Mabey, D. B., "Beyond the Buffet Boundary," *Aeronautical Journal*, Vol. 3, April 1973, pp. 201–215.

[5]Erickson, G. E., and Brandon, J. M., "On the Nonlinear Aerodynamics and Stability Characteristics of a Generic Chine-Forebody Slender Wing Fighter Configuration," AIAA Paper 87-2617, Jan. 1987.

[6]Norris, M. H., and Lan, C. E., "An Experimental Investigation of the Effects of the Leading-Edge Extension and Forebody Flow Separators on the Forebody-Vortex Induced Aerodynamics of a Generic Fighter Configuration," AIAA Paper 91-3251-CP, 1991, pp. 381–389.

[7]Roach, R. A., and Kuhlman, J. M., "Strake Vortex Control Using Pneumatic Blowing," AIAA Paper 91-3274, 1991.

[8]Ng, T. T., Ong, L. Y., Suarez, C. J., and Malcolm, G. N., "Wing Rock Suppression Using Forebody Vortex Control," AIAA Paper 91-3227, 1991.

[9]Bradley, R. G., and Wray, W. O., "A Conceptual Study of Leading-Edge Vortex Enhancement by Blowing," *Journal of Aircraft*, Vol. 11, No. 1, 1974, pp. 33–38.

[10]Campbell, J. F., "Augmentation of Vortex Lift by Spanwise Blowing," *Journal of Aircraft*, Vol. 13, No. 9, 1976, pp. 727–732.

[11]Kuo, C. H., and Lu, N. Y., "Vortex Characteristics over Delta Wing Subject to Transient Along-Core Blowing," *AIAA Journal*, Vol. 33, No. 12, 1995, pp. 2418–2420.

[12]Shi, Z., Wu, J. M., and Valkili, A. D., "An Investigation of Leading-Edge Vortices on Delta Wing with Jet Blowing," AIAA Paper 87-0330, Jan. 1987.

[13]Karagounis, T., Maxworthy, T., and Spedding, G. R., "Generation of Separated Vortices over a Delta Wing by Means of Leading-Edge Flaps," AIAA Paper 89-0997, March 1989.

[14]Rinoie, K., and Stollery, J. L., "Experimental Studies of Vortex Flaps and Vortex Plates," *Journal of Aircraft*, 1994, Vol. 31, No. 2, pp. 322–329.

[15]Marchman, J. F., "Aerodynamics of Inverted Leading-Edge Flaps on Delta Wings," *Journal of Aircraft*, Vol. 18, No. 12, 1981, pp. 1051–1067.

[16]Reddy, C. S., "Effect of Leading-Edge Vortex Flaps on Aerodynamic Performance of Delta Wings," *Journal of Aircraft*, Vol. 18, No. 9, 1981, pp. 796–798.

[17]Wu, J. M., and Wu, J. Z., "Vortex Lift at Very High Angle-of-Attack with Massively Separated Unsteady Flow," IUTAM Symposium on Fluid Dynamics of High Angle of Attack (Tokyo, Japan), 1992, pp. 35–63.

[18]Lamar, J. E., and Campbell, J. F., "Vortex Flaps—Advanced Control Devices for Super Cruise Fighter," *Aerospace America*, Jan. 1984, pp. 95–99.

[19]Deng, Q., and Gursul, I., "Effect of Leading-Edge Flaps on the Vortices and Vortex Breakdown," *Journal of Aircraft*, Vol. 33, No. 6, 1996, pp. 1079–1086.

[20]Campbell, J. F., and Osborn, R. F., "Leading-Edge Vortex Research: Some Non-Planar Concept and Current Challenges," *Vortex Flow Aerodynamics*, Vol. 1, NASA CP-2416, July 1986, pp. 31–63.

[21]Hussain, A. K. M. F., and Reynolds, W. C., "The Mechanics of an Organized Wave in Turbulent Shear Flow," *Journal of Fluid Mechanics*, Vol. 41, Pt. 2, 1970, pp. 241–258.

[22]Reynolds, W. C., and Carr, L. W., "Review of Unsteady, Driven, Separated Flows," AIAA Paper 85-0527, 1985.

[23]Huyer, S. A., Robinson, M. C., and Luttger, M. V., "Unsteady Aerodynamics Loading Produced by a Sinusoidal Oscillating Delta Wing," *Journal of Aircraft*, Vol. 29, No. 3, 1992, pp. 366–373.

[24]Gu, W., Robinson, O., and Rockwell, D., "Control of Vortices on a Delta Wing by Leading-Edge Injection," *AIAA Journal*, Vol. 31, No. 7, 1993, pp. 1177–1186.

[25]Hsu, C. W., "Experimental Investigation of Vortex Structure Above Delta-wing with Leading-Edge Flap," M.S. Thesis, Dept. of Mechanical Engineering, National Chung Hsing Univ., Taichung, Taiwan, ROC, 1996.

[26]Garg, A. K., and Leibovich, S., "Spectral Characteristics of Vortex Breakdown Flow Fields," *Physics of Fluids, Series A*, Vol. 22, No. 11, 1979, pp. 2053–2064.